Turkish Journal of Electrical Engineering & Computer Sciences

http://journals.tubitak.gov.tr/elektrik/

Research Article

Turk J Elec Eng & Comp Sci
(2019) 27: 3967 – 3979

doi:10.3906/elk-1811-197

Investigation of start-up conditions on electric submersible pump driven with flux switching motor

Mohammad Hossein BARZEGARI BAFGHI, Abolfazl VAHEDI*
Department of Electrical Engineering, Center of Excellence for Power System Automation and Operation,
Iran University of Science and Technology, Tehran, Iran

Received: 30.11.2018 • **Accepted/Published Online:** 24.05.2019 • **Final Version:** 18.09.2019

Abstract: One of the motor types that is recently considered to be a candidate for electric submersible pumps (ESPs) is the flux switching motor. Therefore, it becomes crucial to verify that this type of motor can stand ESP conditions. The main subject of this paper is to investigate the start-up condition of ESP along with considering the long power supply cable to study the motor performance, where the real aspect of the ESP conditions is investigated. Since there is not any model of pump load that models the dynamic behavior of ESP correctly, first, a model for the pump is developed. Then the flux switching motor model is modified to apply the long cable to the model. The model is simulated and the results are presented. The main advantages of this paper are modeling the height change of fluid, pump efficiency, and pump load torque during the time (from start to steady state when the flow rate of fluid outcome from the well is stable), and considering the long cable. In addition, the flux switching motor model is validated by a built prototype motor.

Key words: Electric submersible pump, load modeling, flux switching motor

1. Introduction

Although a major amount of oil and gas are currently obtained from wells due to the natural pressure of the reservoirs, in many cases, the reservoir pressures are not sufficient. Therefore, it is necessary to use an artificial lift method to obtain the desired production rate [1]. There are several artificial lift methods, such as sucker rod pump [2], gas injections [3], hydraulic jet pump [4], progressive cavity pump (ESPCP) [5], and electric submersible pump (ESP) [3]. Among these methods, ESP is the most efficient and economical (based on cost per barrel) especially for offshore production [6].

The ESP consists of several components, which may be installed either on the ground surface or the well (subsurface). For example, the motor controller (or variable speed drive), transformer, surface electric cable, and protection systems are usually installed on the ground surface. However, the centrifugal pump, electric motor, seal electric cable, gas separator, sensors, and valves are subsurface components [7]. In Figure 1 a typical ESP is illustrated.

The electric motor has an important role in the ESP system. Three-phase and two-pole squirrel-cage induction motors (IMs) have been used in ESP systems as a traditional and only choice for many years [8, 9]. Other motor types were not appropriate for working under harsh conditions of ESPs, especially at high temperature. Recently advanced technology and materials are developed, which make other electric motors

*Correspondence: avahedi@iust.ac.ir

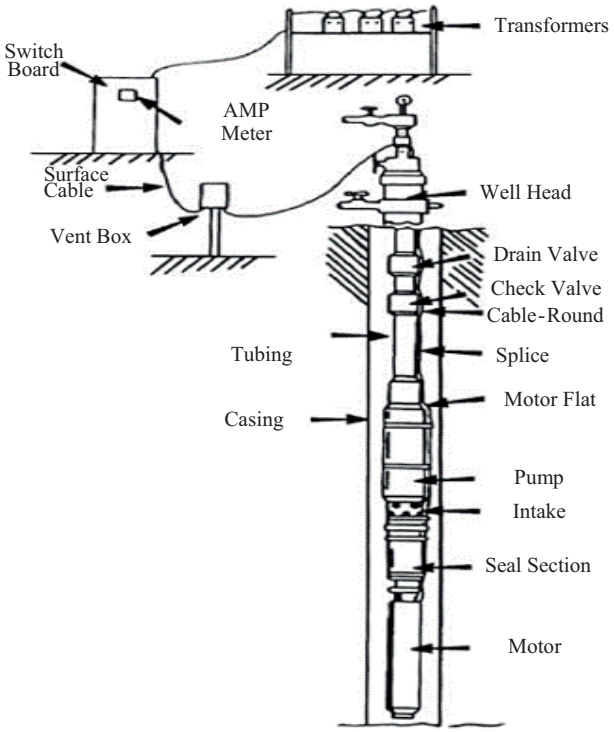

Figure 1. Schematic of an ESP installation [7].

suitable at high temperature. Therefore, recently, interior permanent magnet motors (IPMs) are used in ESPs for some wells.[1] Also, some studies recommended using flux switching motors on ESPs [10, 11].

The flux switching permanent magnet (FSPM) motors have many advantages. PMs and armature coils are placed on the stator in flux switching motors, which leads to the robustness of the rotor, no need to protect PMs again centrifugal force, reduction in the operation temperature of PMs, and reduction in the armature effect on PMs since the fields of coils are perpendicular to PM fields [11]. Nevertheless, a significant concern is about starting and reaching nominal rotational speed in ESP applications.

The ESP system load simulation and starting were investigated in some works, they did not cover the whole process. The authors of [12] investigated the performance of an induction motor for ESP. They simulated the operation of the ESP only for 0.6 s, they did not consider the cable voltage drop for modeling, and they focused on mechanical stress on shaft. The authors of [13] studied the interior permanent magnet motor drive for ESP. They simulated the ESP only for 5 s and assumed the height of fluid was equal to the nominal head for any speed at any moment including starting, and also the cable voltage drop was ignored. The authors of [1] focused on a hysteresis interior permanent magnet motor drive for ESP; they simulated ESP only for 10 s and also assumed the height of fluid was equal to the nominal head for any speed at any moment and also the cable voltage drop was ignored. There is no investigation where the performance of flux switching was studied in ESP systems. In addition, there is no study on long-term performance of ESP load from starting to steady state of the pump. Indeed, when the motor of the ESP is started and reaches its nominal speed, the fluid does not reach the surface, and this procedure needs a long time to be done. Since the torque relates to the flow rate

[1]Borets Corporate Brochure, http://borets.com/about/brochures/

and height of fluid over the pump, it is necessary to consider a practical aspect of load model for simulation of the motor for evaluation.

In this paper a model is developed to consider the dynamic starting, in which several starting conditions are taken into account, such as the initial height of fluid and different pressures on the well head and well bottom. In addition, by the model the height of fluid over the pump can be obtained at any moment before or at steady state. Along with modeling the ESP load, the model of the flux switching motor is presented and the long power supply cable is modeled. Therefore, the evaluation of the motor here is based on practical and real aspects. To evaluate it, the behavior of the flux switching motor supplying the torque of the modeled load and supplied by a long cable is investigated from starting to steady state (when the well output becomes stable). Also, a prototype of a flux switching motor is built to find the voltage and current waveform so that the FSPM model can be verified.

2. ESP model

The ESP is a centrifugal pump. Therefore, the base of the ESP motor load model is the centrifugal pump model. For this type of pump, the following rules exist according to the affinity laws [14, 15]:

- The maximum flow rate of the pump is directly proportional to rotation speed.
- The maximum height that fluid can be pumped (head) is related to the square of rotation speed as in (1) where $H_{\max}$, K_h, and ω are pump head, head coefficient, and rotation speed, respectively.
- The efficiency of the pump does not change with speed change.

$$H_{\max} = K_h \times \omega^2 \tag{1}$$

A typical performance curve of a centrifugal pump is illustrated in Figure 2.

These curves are for almost the steady state of the pump and it is not possible to use them directly for dynamic analysis. There are some relations developed to simulate the transient mode of the pump.

Generally, the height of the liquid column above the pump can be written as a function of flow rate and the initial height as in (2) when H_z, H_i, Q, and A_{Pipe} are height of fluid over pump, initial height of fluid, flow rate, and pipe cross-section area, respectively. This equation makes this model different from other models used in previous literature that modeled ESP load. To modify the height of the fluid, which will be effective in pump operation, a parameter named height loss is defined by (3) where $Coe_{friction}$ is friction coefficient. Then the effective height of fluid can be obtained from (4).

If the pressure in the bottom of the well and the surface are equal, the pump head, liquid height, and flow rate are related together by (5) [16], where a, g, and L_{Pipe} are pump constant, gravity, and length of pipe, respectively. However, if the pressure in the bottom differs from the pressure in the surface, (5) is corrected as (6) while ΔP and ρ are the amount of pressure difference and fluid density, respectively.

$$H_z = H_i + \int \frac{Q}{A_{Pipe}} dt \tag{2}$$

$$H_{loss} = H_z \times Coe_{friction} \times sign\,(Q) \tag{3}$$

$$H_{act} = H_z + H_{loss} \tag{4}$$

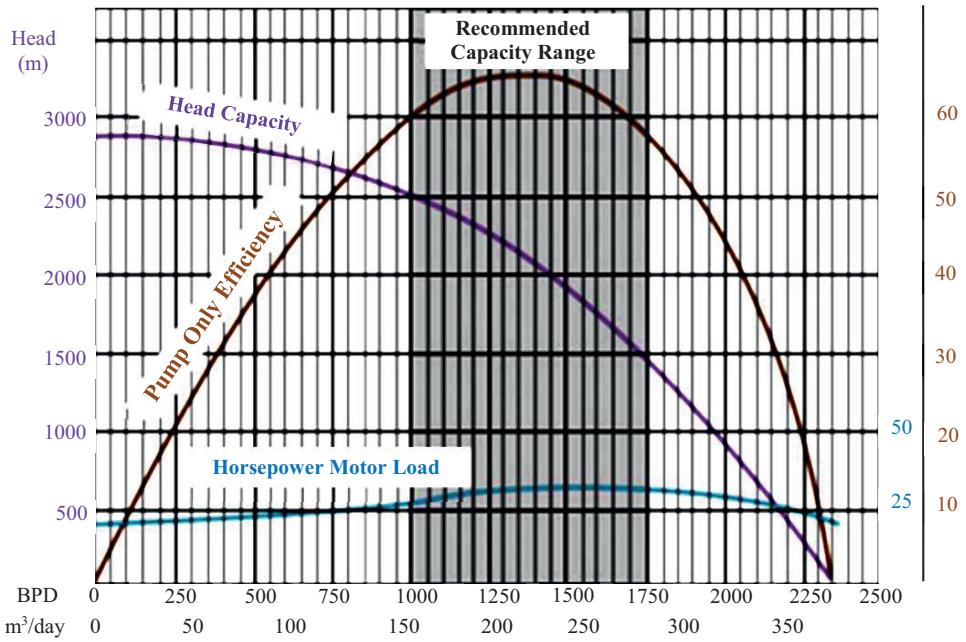

Figure 2. Characteristics of selected pump to be simulated [14].

$$H_{\max} = H_{act} + a \times Q \times |Q| + \frac{L_{Pipe}}{g \times A_{Pipe}} \frac{dQ}{dt} \tag{5}$$

$$H_{\max} = H_{act} + a \times Q \times |Q| + \frac{\Delta P}{\rho} + \frac{L_{Pipe}}{g \times A_{Pipe}} \frac{dQ}{dt} \tag{6}$$

Finally, the pump torque is obtained from (7). Then, based on performance curves of the centrifugal pump, the pump efficiency can be obtained and the motor load torque can be calculated as in (8).

$$T_{Pump} = \frac{\rho \times g \times H_{act} \times Q}{\omega} \tag{7}$$

$$T_{motor} = \frac{T_{Pump}}{Eff_{Pump}} \tag{8}$$

3. FSPM motor model

The flux switching motor model in qd0 coordination is a desired model for simulating starting transient state and steady state. The inductances in d and q axes can be obtained from (9) and (10), where L_q, L_d, L_0, L_m, and L_{sl} are q-axis inductance, d-axis inductance, zero sequence inductance, mutual inductance, and leakage inductance, respectively.

$$L_q = \frac{3}{2}(L_0 + L_m) + L_{sl} \tag{9}$$

$$L_d = \frac{3}{2}(L_0 - L_m) + L_{sl} \tag{10}$$

The total flux linkage in d and q axes is obtained as in (11), where ψ_d, ψ_q, ψ_m, I_d, and I_q are d-axis flux-linkage, q-axis flux-linkage, PM flux-linkage, d-axis current, and q-axis current.

$$\begin{cases} \psi_d = \psi_m + L_d I_d \\ \psi_q = L_q I_q \end{cases} \tag{11}$$

The dq voltages can be written as in (12), where u_d, u_q, ω_e, and R_s are d-axis voltage, q-axis voltage, electrical rotation speed, and phase resistance, respectively.

$$\begin{cases} u_d = \frac{d\psi_d}{dt} - \omega_e \psi_q + R_s I_d \\ u_q = \frac{d\psi_q}{dt} + \omega_e \psi_d + R_s I_q \end{cases} \tag{12}$$

Then the electromagnetic torque can be obtained from (13), where P_r is rotor pole number.

$$T = \frac{3}{2} P_r \left(\psi_m I_q + (L_d - L_q)\, I_q I_d\right) \tag{13}$$

3.1. Long feed cable effect model

As can be seen in Figure 1, the electric motor in the ESP system works underground and its power supply components are on the ground surface. Therefore, the power supply components are far from the electric motor and so the supply cable is long. The long cable causes voltage drop from the power supply to electric motor [17, 18]. This voltage drop is very large for induction motors, which can even prevent the starting of the motor [14]. The long cable can be modeled as series inductance and resistance that are in serial with the electric motor. Therefore, the motor model is modified as below to take the series impedance of the long cable into account while L_f and R_f are cable feed inductance and resistance, respectively.

$$L'_q = L_q + L_f = \frac{3}{2}(L_0 + L_m) + L_{sl} + L_f \tag{14}$$

$$L'_d = L_d + L_f = \frac{3}{2}(L_0 - L_m) + L_{sl} + L_f \tag{15}$$

$$\begin{cases} \psi'_d = \psi_m + L'_d I_d \\ \psi'_q = L'_q I_q \end{cases} \tag{16}$$

$$\begin{cases} u'_d = \frac{d\psi'_d}{dt} - \omega_e \psi'_q + (R_s + R_f)\, I_d \\ u'_q = \frac{d\psi'_q}{dt} + \omega_e \psi'_d + (R_s + R_f)\, I_q \end{cases} \tag{17}$$

3.2. Experimental results

Before simulation a built permanent magnet flux switching motor is tested to verify the model. The electric motor is illustrated in Figure 3 and a sample of test results is shown in Figure 4. The experimental results validated the flux switching motor model. Therefore, it can be used in ESP simulation.

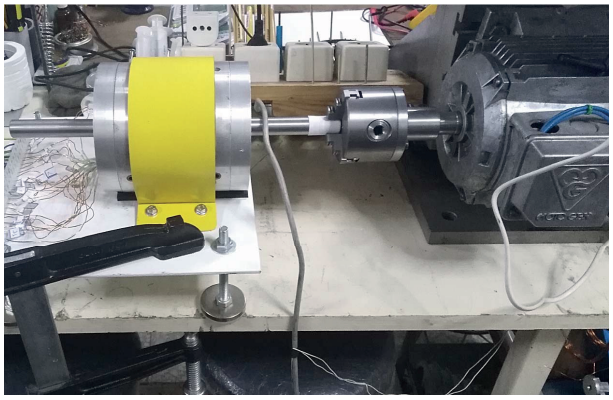

Figure 3. A permanent magnet flux switching motor that is tested.

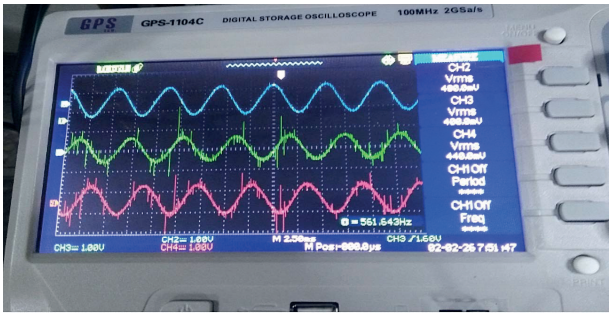

Figure 4. Tested flux switching motor current.

4. Simulation and results

In order to simulate the motor in the ESP system, real pump data are needed to model the pump since the pump efficiency varies for different pumps and can be obtained by experimental results. Therefore, a pump is selected from [14] that has characteristics as in Figure 2. The efficiency function of this pump has been extracted as a fifth-order polynomial as in (18). In this paper SI units are used. Therefore, the parameters of (18) are found in SI units and are presented in Table 1.

$$Eff_{Pump} = \mathrm{C}_1 \times \mathrm{Q}^5 + \mathrm{C}_2 \times \mathrm{Q}^4 + \mathrm{C}_3 \times \mathrm{Q}^3 + \mathrm{C}_4 \times \mathrm{Q}^2 + \mathrm{C}_5 \times \mathrm{Q} + \mathrm{C}_6 \tag{18}$$

Table 1. Pump efficiency parameters.

Parameter	Value	Parameter	Value	Parameter	Value
C_1	-3.621×10^{12}	C_3	-1.286×10^{8}	C_5	354.1
C_2	3.449×10^{10}	C_4	122800	C_6	0.0112

The parameters of the well and motor are illustrated in Table 2.

Table 2. Parameter specifications in simulation.

Parameter	Value	Parameter	Value	Parameter	Value
$\mathrm{L}_d(mH)$	14.308	$\psi_m(wb)$	1.494	$\rho\ \left({}^{Kg}/_{m^3}\right)$	850
$\mathrm{L}_q(mH)$	15.533	P_r	10	$\mathrm{Coe}_{friction}$	0.1
$\mathrm{R}_s(\Omega)$	1.43	$A_{Pipe}\ (m^2)$	0.02545	K_h	0.03
$\mathrm{L}_f(mH)$	0.6096	$\omega_n\ \left({}^{Kg}/_{m^3}\right)$	100π	a	152781081
$\mathrm{R}_f(\Omega)$	1.7	$\mathrm{H}_{well}(m)$	2000	-	-

The ESPs are protected with unidirectional valves and a bypass path for fluid reverse flow. Therefore the initial height of fluid over the pump will be zero. The model is implemented in MATLAB Simulink. The schematics of the pump model and ESP system model are illustrated in Figure 5 and Figure 6, respectively.

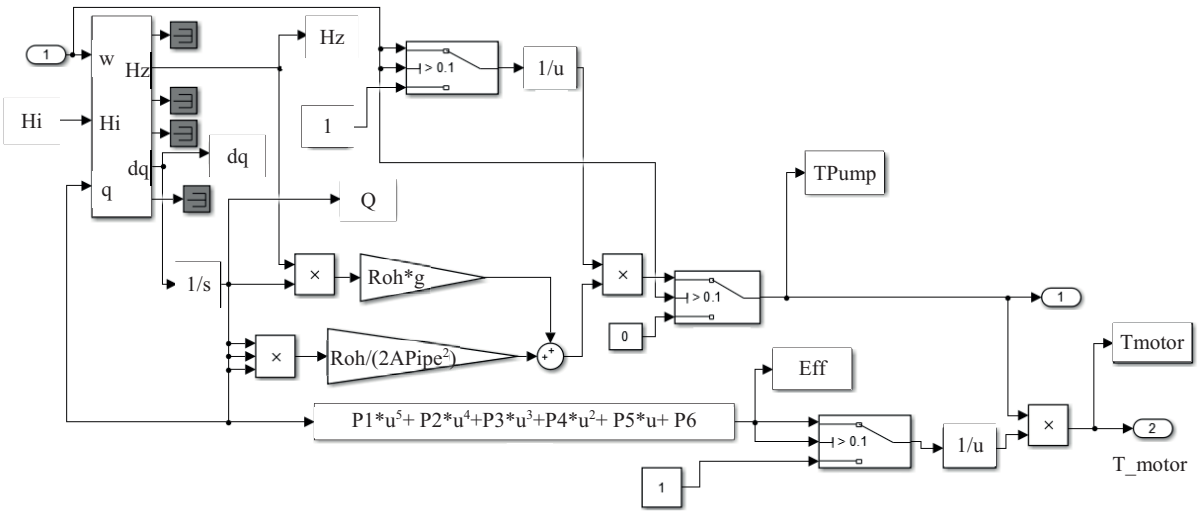

Figure 5. Schematics of pump model (ESP Load Sim).

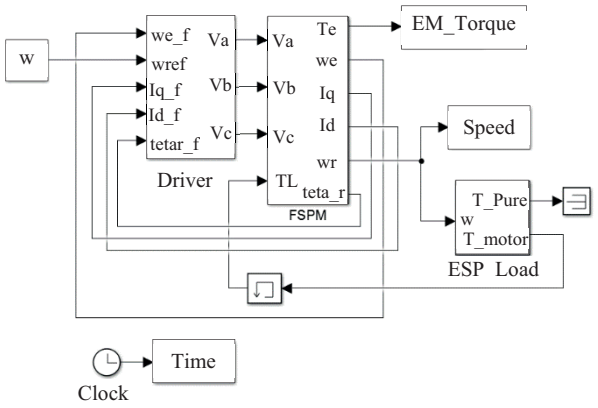

Figure 6. Schematics of the ESP system model in Simulink/MATLAB.

The model is simulated and it is found that the fluid comes out from the well after about 15800 s. After that, the dynamics of the ESP system will not change. However, it must be mentioned that the dynamics of the ESP can divided into three steps:

- Start up
- Speed up
- Increasing height

In the start-up step, it is expected that the current and voltage drop on the cable are large. Also, it is expected that the duration of this step is small (some tenths of a second). If the motor cannot go to the next step, it is called failure. After the start-up step, rotation speed increases to about nominal speed. In this step, a supply voltage increment is expected since the electromotive force relates to the speed. The duration of the speed-up step should be about a few seconds. Likewise, in the speed-up step, if the motor cannot go to the next step, it is called failure. After the speed-up step, the speed will be almost constant, the height of fluid will

slowly increase, and the flow rate will slowly diminish. Also, the input current will slowly increase. Thus, input power will increase. Duration of this step is relatively long (more than several thousand seconds). If the motor cannot provide the maximum power, it will fail.

The total simulation time is 16000 s. When the plots are drawn for total time, only the ESP behavior of the final step can be seen. Therefore, to investigate the ESP behavior of any steps, results are drawn in various time intervals.

The input current is very large at first, but it reduces very fast. The currents on d and q axes are shown in Figure 7 and Figure 8, respectively, for wider time intervals than start-up time. These figures show that the current reduces when the ESP starts. It is concluded that the flux switching motor successfully passed the first step. The rotation speed, flow rate, and height of fluid in this time interval are illustrated in Figure 9, Figure 10, and Figure 11, respectively. As can be seen, rotation speed and flow rate increase due to rotation speed increment. Also, the height of fluid increases but the rate of height increment is low and after 600 ms the height increases about 7 cm according to Figure 11. The pump efficiency is a function of flow rate and becomes maximum when the flow rate is optimized. The input voltage and voltage drop on the cable of phase 1 are illustrated on Figure 12 and Figure 13, respectively.

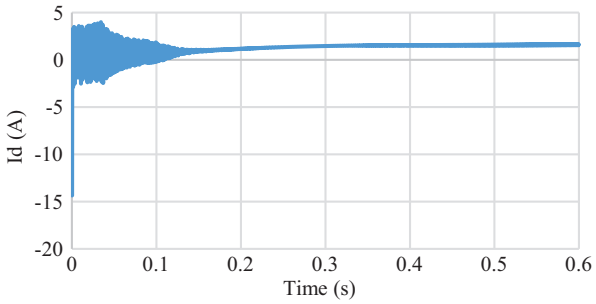

Figure 7. I_d on a wider interval than start-up time.

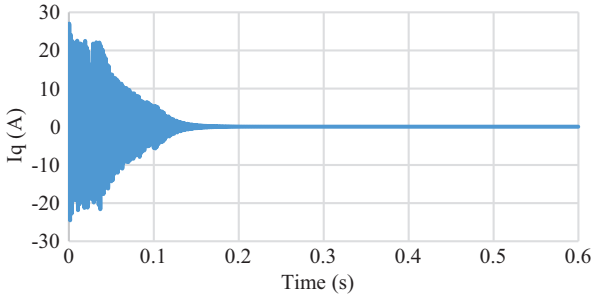

Figure 8. I_q on a wider interval than start-up time.

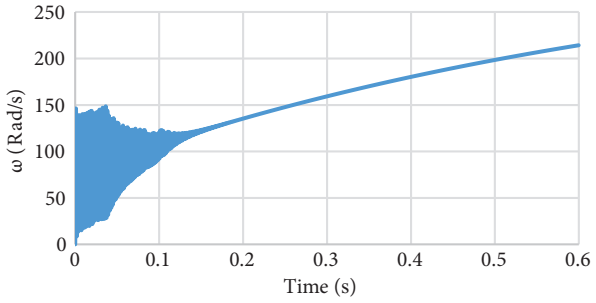

Figure 9. Rotation speed on a wider interval than start-up time.

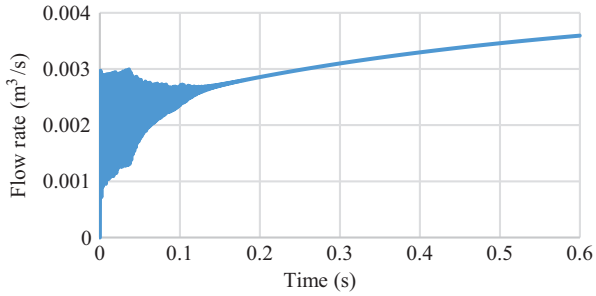

Figure 10. Flow rate on a wider interval than start-up time.

As can be seen, voltage drop on the cable relates to the current amplitude and the proportion of voltage drop on the cable to input voltage is large at first, but it reduces very fast. The speed-up step finishes and an increasing height step starts about 3 s after the motor starts (Figure 14). After that, input voltage will remain constant (Figure 15). The pump load torque is a function of height and flow rate and seems nearly linear during start-up and speed-up (Figure 16). In addition, the motor load torque is a function of the pump load torque and pump efficiency. The pump load torque and motor load torque curve are shown in Figure 16 and Figure 17,

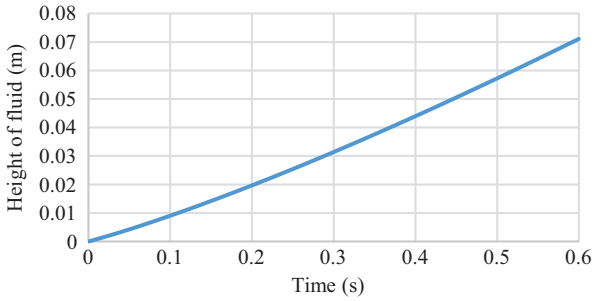

Figure 11. Height of fluid on a wider interval than start-up time.

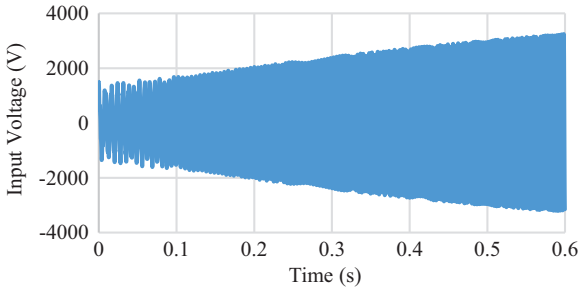

Figure 12. Input voltage of phase 1 on wider interval than start-up time.

respectively. These curves shows that height of fluid is the most effective parameter on torque load in these steps.

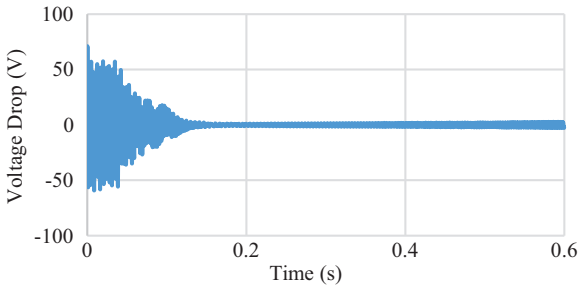

Figure 13. Voltage drop on cable of phase 1 on wider interval than start-up time.

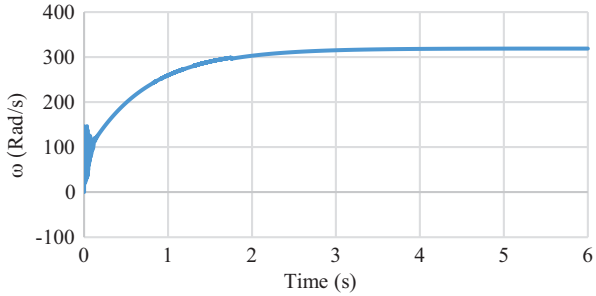

Figure 14. Rotation speed on wider interval than speed-up time.

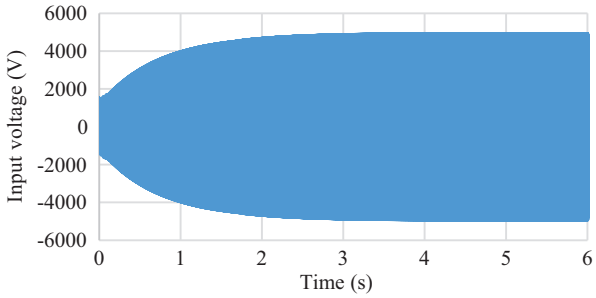

Figure 15. Input voltage of phase 1 on wider interval than speed-up time.

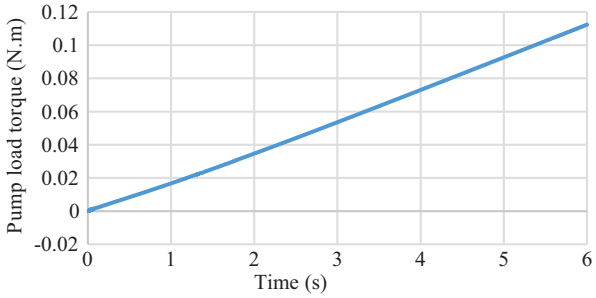

Figure 16. Pump load torque on wider interval than speed-up time.

The cable voltage drop (Figure 18) reduces and the input voltage increases (Figure 15) in the two first steps. Therefore, the proportion of cable voltage drop to input voltage will be negligible.

The simulation shows that flow rate correlates with rotation speed at first (Figure 19 and Figure 20), since the height is very low (Figure 21). However, when the height increases significantly after a while (Figure 22), flow rate reduces (Figure 23).

The pump load torque is a function of flow rate multiplied by the height of fluid over the pump (as in (7)). Therefore, the pump load torque is similar to a second-order equation and has a maximum point (as seen in Figure 24). The motor load torque is the proportion of the pump load torque to the pump efficiency ratio.

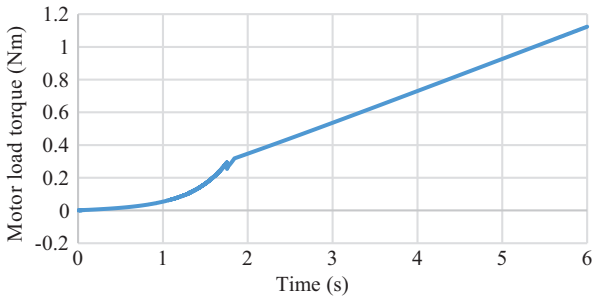

Figure 17. Motor load torque on wider interval than speed-up time.

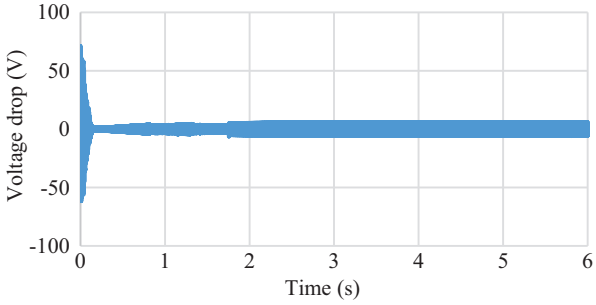

Figure 18. Cable voltage drop on wider interval than speed-up time.

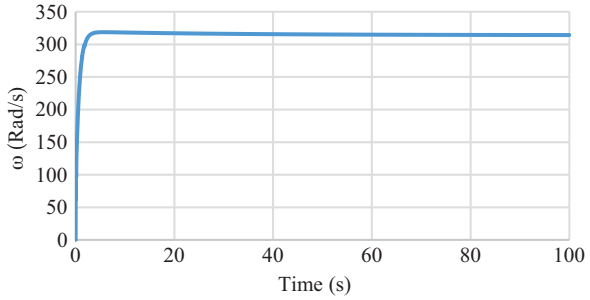

Figure 19. Rotation speed in first 100 s

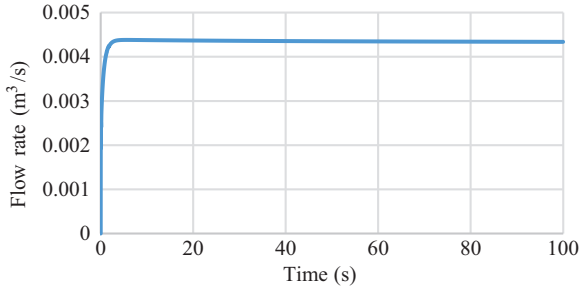

Figure 20. Flow rate in first 100 s.

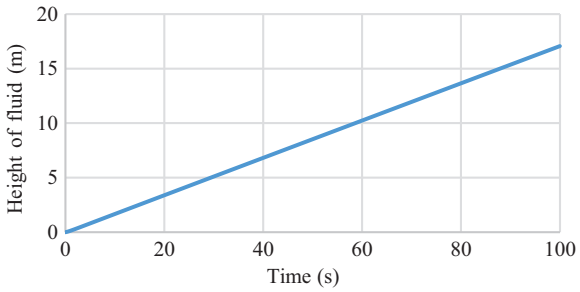

Figure 21. Height of fluid in first 100 s.

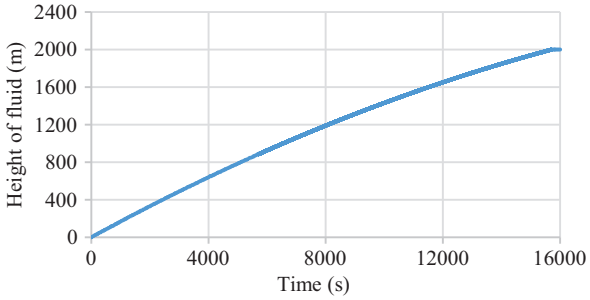

Figure 22. Height of fluid curve from start to stable condition.

The pump efficiency is a function of flow rate whose curve is obtained and presented in Figure 25. The motor load torque is illustrated in Figure 26. The load torque is maximum before the stable point.

Since the 3-phase current is an alternating wave, currents on dq can be more suitable. The Iq and Id are shown in Figure 27 and Figure 28, respectively. The q-axis current Iq waveform is very similar to the motor load torque while the d-axis current (Id) damps from starting to stable condition and finally will be about zero.

To verify the results, the height of fluid vs. flow rate is shown in Figure 29 to be compared with characteristics of the simulated pump. This curve consists of a line that is very close to the horizontal axis. It relates to start-up and speed-up steps in which speed changes from zero to the maximum value and consequently the flow rate increases from zero to maximum, too. These steps take very little time, which leads the height of fluid over the pump to be very small. Indeed, as can be seen in Figure 21, the height of fluid is less than 1 m when the speed reaches the maximum value. The second section of the curve in Figure 29 is very similar to characteristics of the simulated pump, but it stops at a height of 2000 m since the well depth is 2000 m.

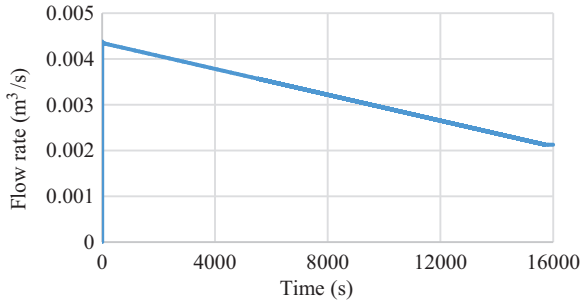

Figure 23. Flow rate curve from start to stable condition.

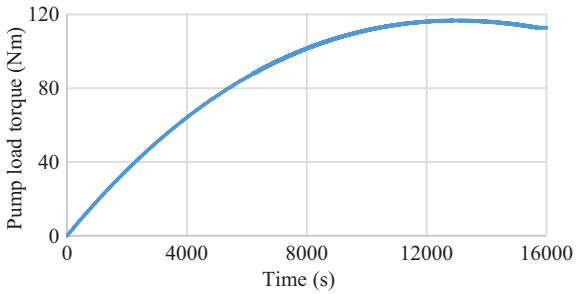

Figure 24. Pump load curve from start to stable condition.

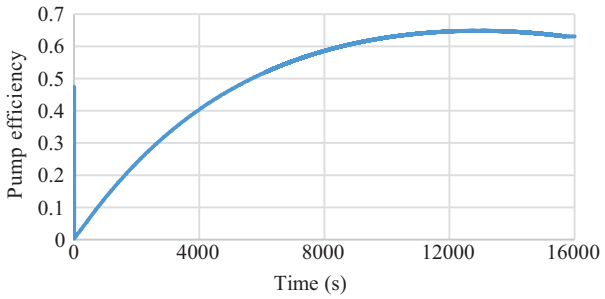

Figure 25. Pump efficiency curve from start to stable head.

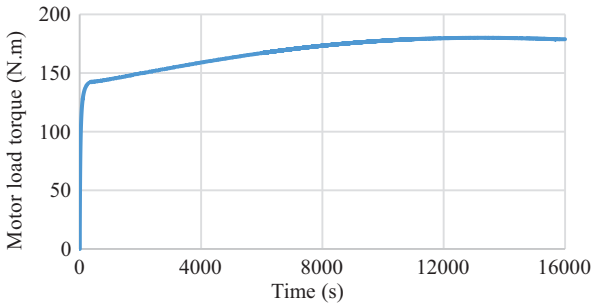

Figure 26. Motor load curve from start to stable condition.

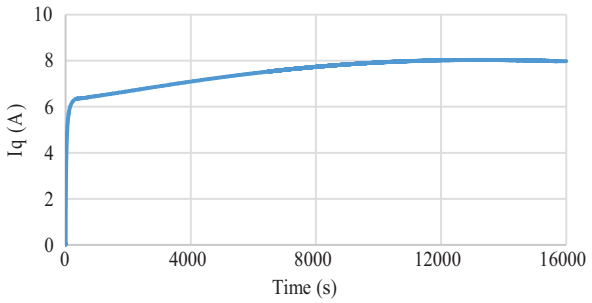

Figure 27. I_q curve from start to stable condition.

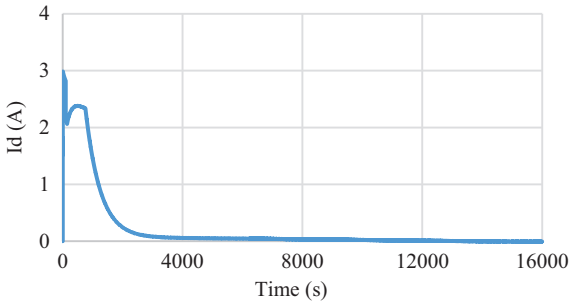

Figure 28. I_d curve from start to stable condition.

To verify the obtained results from the simulated model, they are compared with the characteristics of the simulated pump (Figure 2).

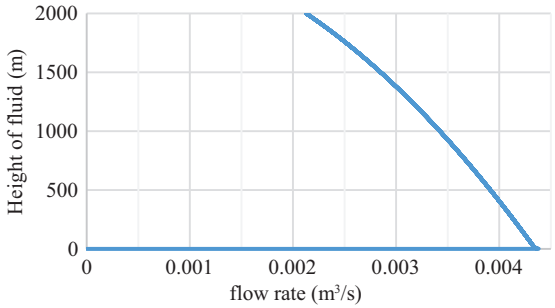

Figure 29. Height of fluid vs. flow rate from start to stable condition.

5. Conclusion

The ESP has drawn researchers' attention recently, and its application in oil wells is growing. On the other hand, FSPM motors have many more advantages than conventional motors for utilization in ESPs. In this paper, the ESP driven by a flux switching motor is modeled. In this model, the effect of long cable power supply, the initial condition of the pump, and other effective parameters are considered. Then the model is simulated, and the simulation results show that the dynamic behavior of the ESP can be divided into three steps. In the first step, the pump starts and it begins to rotate. Second, the pump speeds up to nominal speed, and third, pump speed becomes constant and fluid flows through the well to surface. When the fluid comes to the surface, the pump becomes stable. The simulation results demonstrate the flow rate, pump load torque, motor load torque, pump efficiency, and other parameters vary from start to stable condition. The maximum point of the motor load torque is not at the beginning of the torque curve and it occurs near the stable point. The current on the q axis is very similar to the motor load torque. The input voltage increases until the rotation speed reaches nominal speed. The portion of the voltage drop on the cable to the input voltage is very large at first, but it reduces very fast. Finally, the simulation results show that the flux switching motor can drive an ESP, and evidently, it will be essential to investigate more details for FSPM motor applications in ESPs for drive system design and control. In addition, the model can be employed for other applications similar to ESPs, such as other centrifugal pumps for any fluid.

References

[1] Rabbi SF, Rahman MA, Sarker MM, Butt SD. Modeling and performance evaluation of a hysteresis IPM motor drive for electric submersible pumps. In: IEEE 2015 Energy Conversion Congress and Exposition (ECCE); Montreal, Canada; 2015. pp. 4105-4112.

[2] Khakimyanov MI, Shafikov IN, Khusainov FF. Control of sucker rod pumps energy consumption. In: International Siberian Conference on Control and Communications; Omsk, Russia; 2015. pp. 1-4.

[3] Fatahi E, Jalalifar H, Pourafshari P, Rostami AJ. Selection of the best artificial lift method in one of the Iranian oil field by the employment of ELECTRE model. British Journal of Applied Science and Technology 2011; 1 (4): 172-180. doi: 10.9734/BJAST/2011/585

[4] Clark C, Kosmicki R. Hydraulic jet pumps prove worth for lifting early production. World Oil 2014. 141-144.

[5] Samuel GR, Saveth KJ. Optimal design of progressing cavity pumps (PCP). Journal of Energy Resources Technology 2006; 128 (4): 275-279. doi: 10.1115/1.2358142

[6] Lea JF, Nickens HV. Selection of artificial lift. In: SPE 1999 Mid-Continent Operations Symposium; Oklahoma City, OK, USA; 1999. pp. 1-30.

[7] Guo B, Lyons WC, Ghalambor A. Petroleum production engineering a computer-assisted approach. Houston, TX, USA: Gulf Professional Publishing, 2007.

[8] Romero OJ, Hupp A. Subsea electrical submersible pump significance in petroleum offshore production. Journal of Energy Resources Technology 2013; 136 (1): JERT-12-1245. doi: 10.1115/1.4025258

[9] Dillard MS, Greiner DT. Transient voltage protection for induction motors including electrical submersible pumps. IEEE Transactions on Industry Applications 1987; 23 (2): 365-370.

[10] Bafghi MHB, Vahedi A. A comparison of different electric motors for electrical submersible pumps used in oil and gas industries. IOP Conference Series Materials Science and Engineering 2018; 433 (1): 012091. doi: 10.1088/1757-899X/433/1/012091

[11] Chen A, Nilssen R, Nysveen A. Investigation of a three-phase flux-switching permanent magnet machine for downhole applications. In: 2010 XIX International Conference on Electrical Machines; Rome, Italy; 2010. pp. 707-711.

[12] Thorsen OV, Dalva M. Combined electrical and mechanical model of electric submersible pumps. IEEE Transactions on Industry Applications 2001; 37 (2): 541-547. doi: 10.1109/28.913720

[13] Rabbi SF, Rahman MA, Butt SD. Modeling and operation of an interior permanent magnet motor drive for electric submersible pump. In: 2014 International Ocean Conference; Washington, DC, USA; 2014.

[14] Takacs G. Electric Submersible Pump Manual: Design, Operations and Maintenance. Houston, TX, USA: Gulf Professional Publishing, 2009.

[15] Karassik IJ, McGuire T. Centrifugal Pump. New York, NY, USA: Chapman and Hall, 1998.

[16] Szymczyk J, Karaskiewicz K. The modeling of centrifugal pump transients. Transactions of the Institute of Fluid-Flow Machinery 2015; 130: 83–92.

[17] Massoud A, Elserougi A, Abdel-Khalik A, Ahmed S. A four-switch based long-cable-fed five-phase induction motor drive system. In: IEEE 2016 Symposium on Computer Applications and Industrial Electronics; Batu Feringghi, Malaysia; 2016. pp. 139-144.

[18] Lewis-Rzeszutek HL, Tallam RM, Phukan R, Solveson M, Clancy T. Simulation of cable charging current and its effects on operation of low power AC drives. In: IEEE 2016 Energy Conversion Congress and Exposition; Milwaukee, WI, USA; 2016. pp. 1-20.